GET: A generic electronics system for TPCs and nuclear physics instrumentation

E.C. Pollacco [a,*], G.F. Grinyer [b,c,*], F. Abu-Nimeh [d], T. Ahn [d,e], S. Anvar [a], A. Arokiaraj [f], Y. Ayyad [d], H. Baba [g], M. Babo [f], P. Baron [a], D. Bazin [d], S. Beceiro-Novo [d], C. Belkhiria [c], M. Blaizot [c], B. Blank [h], J. Bradt [d,i], G. Cardella [j], L. Carpenter [d], S. Ceruti [f], E. De Filippo [j], E. Delagnes [a], S. De Luca [j,k], H. De Witte [f], F. Druillole [h], B. Duclos [c], F. Favela [j], A. Fritsch [l], J. Giovinazzo [h], C. Gueye [c], T. Isobe [g], P. Hellmuth [h], C. Huss [h], B. Lachacinski [h], A.T. Laffoley [c], G. Lebertre [c], L. Legeard [c], W.G. Lynch [d,i], T. Marchi [f], L. Martina [c], C. Maugeais [c], W. Mittig [d,i], L. Nalpas [a], E.V. Pagano [m,n], J. Pancin [c], O. Poleshchuk [f], J.L. Pedroza [h], J. Pibernat [h], S. Primault [c], R. Raabe [f], B. Raine [c], A. Rebii [h], M. Renaud [f], T. Roger [c], P. Roussel-Chomaz [a], P. Russotto [m], G. Saccà [j], F. Saillant [c], P. Sizun [a], D. Suzuki [g], J.A. Swartz [f,o], A. Tizon [h], A. Trifiró [j,k], N. Usher [d], G. Wittwer [c], J.C. Yang [f,p]

[a] CEA Irfu, Centre de Saclay, 91191 Gif-sur-Yvette, France
[b] Department of Physics, University of Regina, Regina, SK S4S 0A2, Canada
[c] Grand Accélérateur National d'Ions Lourds (GANIL), CEA/DSM-CNRS/IN2P3, Bvd Henri Becquerel, 14076 Caen, France
[d] National Superconducting Cyclotron Laboratory, Michigan State University, East Lansing, MI 48824, USA
[e] Department of Physics, University of Notre Dame, Notre Dame, IN 46556, USA
[f] KU Leuven, Instituut voor Kern- en Stralingsfysica, 3001 Leuven, Belgium
[g] RIKEN Nishina Center, 2-1 Hirosawa, Wako, Saitama, 351-0198, Japan
[h] Centre d'Études Nucléaires de Bordeaux Gradignan, Université Bordeaux 1, UMR 5797 CNRS/IN2P3, Chemin de Solarium, BP 120 33175, Gradignan, France
[i] Department of Physics and Astronomy, Michigan State University, East Lansing, MI 48824, USA
[j] INFN, Sezione di Catania, Catania, Italy
[k] Dipartimento di Scienze MIFT, Università di Messina, Messina, Italy
[l] Department of Physics, Gonzaga University, Spokane, WA 99258, USA
[m] INFN, Laboratori Nazionali del Sud, Catania, Italy
[n] Dipartimento di Fisica, Università di Catania, Catania, Italy
[o] Department of Physics and Astronomy, Aarhus University, DK 8000, Aarhus C, Denmark
[p] Physique Nucléaire Théorique, Université Libre de Bruxelles, B-1050 Brussels, Belgium

ARTICLE INFO

ABSTRACT

General Electronics for TPCs (GET) is a generic, reconfigurable and comprehensive electronics and data-acquisition system for nuclear physics instrumentation of up to 33792 channels. The system consists of a custom-designed ASIC for signal processing, front-end cards that each house 4 ASIC chips and digitize the data in parallel through 12-bit ADCs, concentration boards to read and process the digital data from up to 16 ASICs, a 3-level trigger and master clock module to trigger the system and synchronize the data, as well as all of the associated firmware, communication and data-acquisition software. An overview of the system including its specifications and measured performances are presented.

1. Introduction

General Electronics for TPCs (GET) is a scalable and generic electronics system that was originally designed for gas-filled detector applications in nuclear physics including Time Projection Chambers (TPCs)

* Corresponding authors.
E-mail addresses: Pollacco@cea.fr (E.C. Pollacco), GF.Grinyer@uregina.ca (G.F. Grinyer).

Table 1

Summary of detector projects worldwide and their total demand in terms of number of GET electronics channels. Applications for the GET system include gaseous detectors (G), auxiliary detectors such as silicon and caesium-iodide detectors (A), as well as beam trackers and beam monitors (T).

Detector project	Application	Country	Channels	Ref.
LAMPS TPC	G	Korea	33792	[2]
ACTAR TPC	G,A	France	20480	[3]
SπRIT	G	Japan	14080	[4]
AT-TPC	G	United States	12800	[5]
HypTPC	G	Japan	8192	[6]
FARCOS	A	Italy	6144	[7]
nTOF	T	Switzerland	4352	[8]
CAT	G	Japan	2816	[9]
ELI-NP TPC	G	Romania	2048	[10]
CAS Lanzhou	G	China	2048	[11]
PANDAX-III	G	China	2048	[12]
SpecMAT	G,A	Belgium	2048	[13]
TexAT	G,A	United States	2048	[14]
Notre Dame	G	United States	1024	[15]
S^3	T	France	1024	[16]
UCAS Beijing	G	China	1024	[17]
Other Projects	G,A,T		2560	
Number of channels worldwide			118528	

and "active targets", which are TPCs where the gas volume is used as both the detection medium and as a thick target to induce secondary nuclear reactions. Some of the key requirements for these types of detection systems in the nuclear physics community (and that are not available with existing commercial electronics) include a high-density front end with a corresponding large number of electronic channels, the need to trigger the system with events from both external (e.g. Si detectors) and internal sources (e.g. total multiplicity), and high-rate data transfer with minimal system dead time. To achieve these goals, we have developed the GET system whose electronics architecture is based on a versatile Application Specific Integrated Circuit (ASIC) design with several modes of acquisition, a 256-channel front-end card with an analog-to-digital converter (ADC), a data concentration system with an embedded Field Programmable Gate Array (FPGA) to improve the rate of the data acquisition and to process data flow from thousands of channels, and a unique three-level programmable trigger. As described below, these developments are essential for realizing many of the experimental programs foreseen with next-generation active target and time projection chamber detection systems in nuclear physics. A recent review of some of the existing and planned detector projects can be found in Ref. [1].

Although GET was initially motivated by gas-filled detectors, the system was designed to be as generic as possible with the intention of using it for other applications. Today, GET is being successfully employed in a growing number of projects using silicon detectors and scintillating detectors such as caesium iodide (CsI), lanthanum bromide (LaBr$_3$) and cerium bromide (CeBr$_3$) for charged-particle and γ-ray spectroscopy. A summary of detector projects that have adopted the GET system and their demand in terms of total number of electronic channels is provided in Table 1.

In this article, an introduction to the different types of physics programs and detection systems that were used to define the conceptual design and specifications of the GET system will be presented in Section 2. A broad and detailed overview of the system architecture will be described in Section 3. Measured performances obtained through several tests performed by users of the GET system and comparisons to the design specifications will be discussed in Section 4. We will then conclude with a brief summary of a select number of detector projects that have adopted the GET system, introduce future projects that could benefit from these developments, and provide an outlook towards possible upgrades of the GET system for future applications.

2. Physics opportunities with GET

Studies of nuclear structure and rare decay modes for the most exotic nuclei, those furthest from stability, are crucial for understanding the origins of matter in the universe, describing the evolution of nuclear forces towards extreme neutron-to-proton ratios, and predicting the onset of new and exotic phenomena. Due to the significant decrease in the production cross sections, access to these nuclei in statistically significant quantities is a fundamental challenge that is continually being addressed through upgrades and construction of large-scale rare-isotope beam accelerators. Even with such powerful facilities, intensities of rare-isotope beams are, and will be, extremely limited and their optical properties (beam size and emittance) will be relatively poor compared to beams of stable ions. Large acceptance detection systems with the highest possible efficiency and inherent spatial and energy resolution are thus essential for providing as much detailed and quantitative spectroscopic information as possible.

Given these challenges, the use of gas-filled time projection chambers and active targets offers an attractive alternative to conventional experimental techniques because of their intrinsic efficiency, spatial resolution, versatility, portability, event-by-event tracking and particle identification capabilities. Operated as an active target, the target thickness (gas pressure) can be increased by orders of magnitude relative to solid foil targets without an appreciable loss in resolution thus compensating, in part, for the low beam intensities. There are several different types of previous generation active targets and TPCs already operating in nuclear physics including IKAR at GSI [18], the MSTPC at RIKEN [19], the MAYA active target at GANIL [20], and the CENBG TPC [21]. Some of the physics highlights from these detectors over the past decade include the discovery of the ground-state resonance in the unbound ^{7}H system [22], studies of neutron-rich halo structure phenomena in ^{11}Li [23,24] and ^{14}Be [25], pioneering studies of giant resonances in unstable Ni isotopes [26,27], and the first direct observation of two-proton radioactivity from the ground states of ^{45}Fe [28] and ^{54}Zn [29].

While extremely successful, many of these detectors suffered from a number of limitations that have prevented them from achieving their full potential. For detectors that track both the incident beam and the (light) reaction products simultaneously, the dynamic range is often a significant challenge. The typical energy loss of the ion beam is on the order of 1 GeV while light products deposit energies of only 1 MeV or less. It is very difficult, if not impossible, to find a common gain that is high enough to observe the light particles without saturating the signals from the beam. A second limitation arises from exceedingly long dead times associated with present data-acquisition systems that significantly reduce the total number of accepted events. In two-proton radioactivity experiments with the CENBG TPC for example, nearly one third of the decay events could not be recorded due to dead-time losses [29]. The lack of an internal trigger option has, until now, further hindered the ability to select only the rare events of interest. Tracking multiple particles following a reaction or decay is also a major challenge for present data-acquisition systems based on analog electronics as signals often overlap on common strips or pixels. Separating the individual contributions from each particle would thus require digital signal processing on a channel-by-channel basis. Another limitation concerns the relatively poor spatial resolution that could be improved with smaller pad sizes or strip pitches. However, as the pixel size decreases, both the total number of electronic channels (cost and complexity) and the overall data throughput (bandwidth and disk space) increases significantly. Present-generation detection systems have thus been limited to approximately 2000 channels or, as in most of the detectors described above, significantly less.

Owing to a large number of recent technological developments in micro-pattern gaseous detectors [30–32], connectors and cables to achieve higher-density point-to-point contacts, and coupled to the achievements made in the GET project in terms of high-density electronics, front-end data processing, and a high-throughput data acquisition

system, next generation active target and TPCs can achieve nearly 25 times higher channel densities than could previously be contemplated. Combined with the unique capabilities of these detectors for certain types of experiments, demands for next-generation active target and TPC detection systems in the nuclear physics community and their needs in terms of electronics and data acquisition have increased dramatically over the last 5 years. The GET system, described below, has confronted these requirements and the result is a state-of-the-art electronics and data-acquisition system for nuclear physics instrumentation of up to 33792 channels.

3. GET system architecture

3.1. System overview

Based on the experience gained with previous active target and TPC detection systems and considering the physics goals for many of the ongoing and emerging detector projects (Table 1), a number of general requirements were identified and included into the final design of the GET system. A schematic overview of the GET system with a single MicroTCA chassis is presented in Fig. 1. Dedicated connectors on the MuTanT module (see Section 3.6) allow up to two additional chassis to be combined to reach a total of 33792 electronic channels. The system design includes all of the hardware, firmware and software from the front-end AsAd cards (Section 3.3) to data acquisition and storage. This development does not include the chassis or the MicroTCA carrier hub (MCH) network switch, both of which are commercially available. Users must provide the interface (cables or interconnection boards) between the detector and the front-end cards. Each of the components presented in Fig. 1 are described in detail in this section.

3.2. AGET: ASIC for GET

The AGET chip is the very front-end of the GET system that performs the first concentration of the data from 64 input channels to one analog output connected to an external ADC. Its architecture is based on the AFTER ASIC [33] but has been improved significantly with new features and modifications to match the different detector requirements (gain and drift time), to discriminate the detector signals (multiplicity signal for building the trigger, hit channel address for selective readout), to decrease the dead time (selective readout, 1 to 512 analog memory cells) and to handle specific physics requirements such as 2-proton radioactivity in the case of the ACTAR TPC project (see below). The AGET chip was fabricated using the AMS 0.35 μm CMOS process. The chip measures 8.5×7.6 mm^2 and is housed in a low quad flat package with 160 pins. The power consumption is less than 10 mW/channel for a 3.3 V power supply. A detailed summary of the AGET specifications are provided in Table 2.

A schematic overview of the AGET architecture is presented in Fig. 2. Each channel integrates a charge-sensitive pre-amplifier (CSA), an analog filter (shaper), an inverting 2× gain (Gain-2) stage, a discriminator for multiplicity building and a 512-cell switch capacitor array (SCA). The pre-amplifier has four different gain settings to support dynamic ranges of 120 fC, 240 fC, 1 pC or 10 pC that can be adjusted on a channel-by-channel basis. The analog filter is formed by a pole-zero cancellation stage followed by a 2-complex pole Sallen–Key low-pass filter. The peaking time of the global filter can be selected from among 16 different values ranging from 70 ns to 1 μs. The filtered signal is then sent to the analog memory and discriminator inputs. The SCA for the analog memory is a 512-cell deep circular buffer in which the analog signal from the shaper is continuously sampled and stored. The sampling frequency is adjustable from 1 MHz to 100 MHz depending on the particular requirements of each detector.

For each channel, the internal pre-amplifier (CSA) stage can be bypassed. Input signals can enter directly into the Sallen–Key low-pass filter or the inverting Gain-2 and discriminator stages. This feature was

Table 2
Specifications of the AGET chip.

Parameter	Specification
Input polarity	Positive or negative
Pre-amplifier	Internal or external
Input dynamic range	120 fC, 240 fC, 1 pC, or 10 pC
Output dynamic range	2 V (peak-to-peak)
Gain	Adjustable channel-by-channel
Discriminator	Leading edge
Input noise level	< 2%
Charge resolution[a]	< 850 e$^-$
Peaking time (16 values)	70 ns to 1 μs
Number of sampling time bins	512
Sampling Frequency	1 to 100 MHz
Time resolution	≤ 20 ns
Threshold	Adjustable channel-by-channel
Zero suppression	Adjustable channel-by-channel
Channel readout mode	Hit, selected or all channels
Power consumption	< 10 mW/channel

[a] Measured with 120 fC dynamic range, 200 ns peaking time and < 30 pF input capacitance.

designed for applications requiring external pre-amplifiers to be coupled to the GET system. A schematic view of the AGET front-end architecture is presented in Fig. 3.

To process two consecutive events within a time window of 2 ms, such as the implantation of a radioactive ion followed by its decay, the SCA memory can be split into two halves using an adjustable parameter in slow control. The first signal that arrives is sampled and stored in the first half of the SCA memory. This is followed by a switch to the second half of the memory to sample and store the second signal. The system waits for this second signal to arrive for up to 2 ms. The switching from one half of the memory to the other corresponds to 2 sampling times.

Sampling is stopped by a trigger decision. In the readout phase, the analog data from the different channels is multiplexed towards a single output and sent to the external 12-bit ADC at a readout frequency of 25 MHz. Three different readout modes are available: all channels, only hit channels, or individually selected channels. It is also possible to read only a user-defined fraction of the 512 analog cells (1 to 512) beginning from an index defined with a constant offset from the cell corresponding to the trigger arrival. The filtered signal, after a differential gain amplification stage, is compared by the discriminator to a threshold value defined by programmable 8-bit digital-to-analog converters. The first four bits (polarity and the 3 most significant bits) are common to all 64 channels while the 4 least significant bits can be fine tuned on a channel-by-channel basis. When the signal crosses the threshold, the discriminator output signal is combined with the other 63 discriminator signals to create a multiplicity signal (analog sum signal) whose duration can be selected to be the time-over-threshold or fixed to a constant value (100 or 200 ns). During the SCA writing phase, the multiplicity signal is continuously digitized by the same external 12-bit ADC used for the SCA readout and is analysed in real time to build a trigger signal. The output signal of the discriminator also sets a temporary hit-channel register at the end of the SCA writing phase.

A serial peripheral interface (SPI) compatible serial link is used to configure all of the AGET-chip parameters through 12 registers with different widths (16 to 128 bits). This link operates at 25 MHz and can also be used to access the hit-channel register (at 50 MHz) through a specific high-speed protocol. The AGET chip includes a test system that uses two dedicated inputs (current and voltage input signals) that are useful for electrical calibration and to test the ASIC functionality for all electronic channels.

In addition to the 64 input signal channels, the AGET chip has 4 channels (channels 11, 22, 45 and 56 when counting all 68 channels from 0 to 67) that are called fixed-pattern noise (FPN) channels. The FPN channels are distributed across the AGET to place one FPN channel on each edge of the chip. The inputs of these channels are not connected to the detector but they are treated by the SCA in exactly the same way
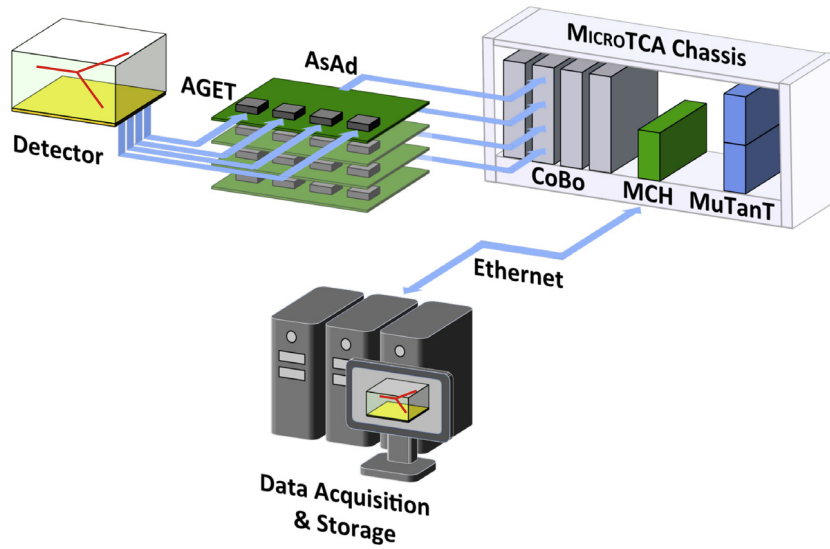
Fig. 1. Schematic overview of the GET system with a single MICROTCA chassis (maximum of 11264 channels). Up to 2 additional MICROTCA chassis can be combined to achieve the maximum system size of 33792 channels. Both the chassis and the MICROTCA carrier hub (MCH) network switch are commercially available. A detailed description of each component is provided in Section 3.
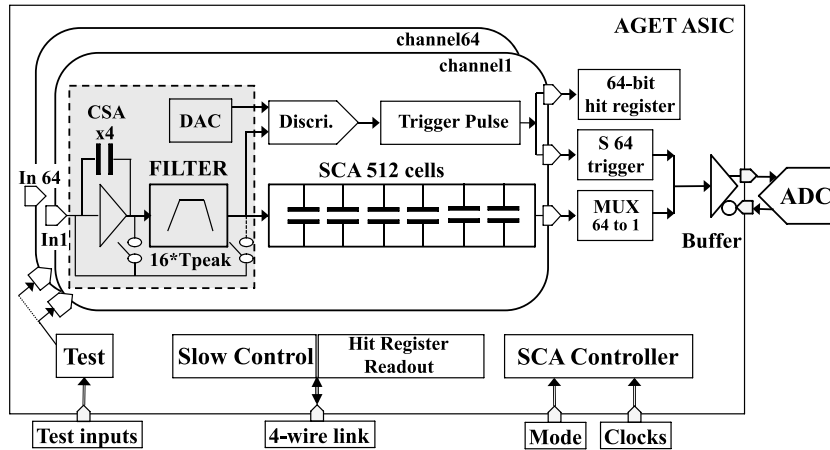

Fig. 2. Architecture of the ASIC for GET (AGET). The dashed-line and shaded area corresponds to the front-end part of the chip that is presented in more detail in Fig. 3.
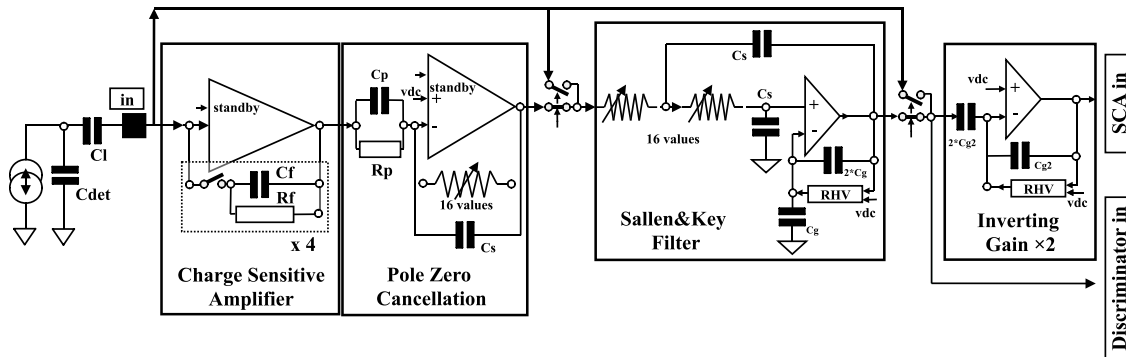
Fig. 3. Schematic overview of the AGET front-end that consists of the charge sensitive amplifier (CSA), the pole zero cancellation (PZC), the Sallen and Key Filter (SK) and the inverting 2× gain (Gain-2) stages. Arrows at the top of the figure indicate which of these stages can be bypassed (selectable via slow control).

as the 64 input signal channels. Data from the FPN channels can be useful offline to determine the intrinsic noise level and baseline shapes in order to improve the overall resolution. A detailed study of raw data samples and the use of the FPN channels for data analysis can be found in Ref. [34].

The AGET design does not include protection against saturation. Signals exceeding the dynamic range of the channel by 10% after the Gain-2 amplification stage will not significantly impact its behaviour. However, if the signal exceeds 200% of the dynamic range, the pre-amplifier will begin to saturate. When saturated, the input impedance increases

dramatically and excess input charge needs to find other ways to flow. One possible charge drain is through parasitic capacitance to adjacent channels (on the chip itself or the detector) that will lead to cross-talk. Saturation will also decrease the voltage of the CSA input. This node is only progressively reloaded by an attenuating current mirror that is limited to 10 nA. The reloading process is therefore long, requiring as much as a few hundred microseconds, during which time the channel is blind and its excess input charge transferred (cross-talk). Once reloaded, the channel itself has recovered but all of the unusual signals and effects caused by this saturation–desaturation process will require additional time to travel through the rest of the chain. Depending on the saturation level, the AGET configuration and the capacitance coupling with the detector, the maximum duration of this process is approximately 1 ms. For some applications, this can represent a limitation that must be taken into account in the analysis of the data. This effect could, in principle, be removed and a study of an external pre-amplifier circuit compatible with AGET is in progress (see Section 6).

3.3. AsAd: ASIC and ADC

The ASIC and ADC (AsAd) board is the front end of the GET system. As shown in Fig. 1, they are located between the detector and the concentration boards described in Section 3.5. The connection between the AsAd board and the different detectors is performed using detector specific adapter cards that may include protection circuits to protect the front-end electronics against sparking. The particular design of these adapter cards and protection circuits are thus very specific to the geometries and connectors chosen for the individual detectors. All of the detector projects listed in Table 1 have therefore designed their own custom boards.

The AsAd board measures 234×160 mm^2. A photograph of a single AsAd card is presented in Fig. 4. The card is powered by a single 3.6 V/1.5 A external power supply. Each AsAd board houses 4 AGET chips and consists of an FPGA (ACTEL ProASIC3E model A3PE1500) and a 4-channel ADC. Each board can therefore process up to 256 analog input signal channels plus the 16 FPN channels. The main tasks of the AsAd board are to process the detector signals through the AGET, digitize the samples stored into the AGET SCA analog memory, and send these digital data to the concentration boards. The AsAd board is slow controlled with five serial ports. Four of these ports are used to control each AGET while the fifth is used for other on-board AsAd devices. All operating parameters are configured and monitored through control and status registers.

For each AGET chip, the signals stored in the memory cells of the SCA (for the channels to be read) are multiplexed and converted in parallel using a 4-channel 12-bit ADC. Signal extraction is performed at a frequency of 25 MHz (the clock from the concentration boards). This clock is duplicated through phase-locked-loop (PLL) cores embedded into the AsAd FPGA in order to phase shift the master readout clock from the concentration boards and to synchronize the sampling of the ADCs with the readout of the SCA. The maximum processing time, obtained for the readout of the full SCA memory (512 cells) of all 68 AGET channels (64 analog signals + 4 FPN channels), is 1.44 ms. The data are then transmitted to the concentration boards with a maximum data rate of approximately 1.2 Gb/s (or 300 Mb/s per AGET). Processing time can be decreased by distributing the hit channels across several AGET chips. Concentrating too many hit channels on a single AGET leads to prohibitively long dead times as described in Section 4.3.

The data extraction and conversion occur after the trigger has been accepted and once the writing in the SCA memory is complete. While the system is in write mode, the multiplicity information (the number of channels exceeding their programmable threshold) issued by the AGET chips is digitized at 25 MHz (independent of the SCA write frequency). The multiplicity information is then sent to the concentration boards and the trigger module (see Section 3.6) where it can be used to generate a trigger decision.
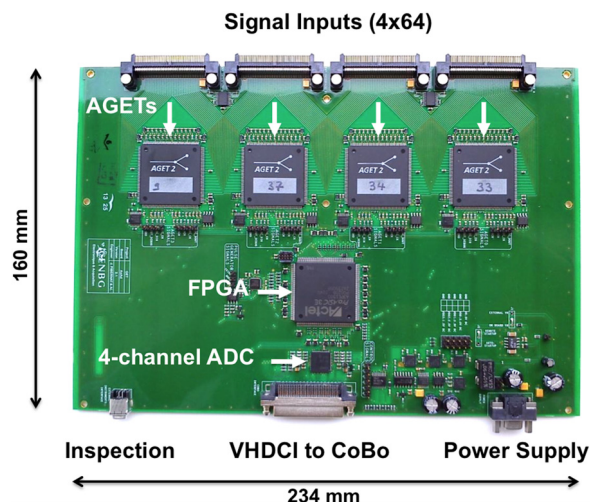

Fig. 4. Photograph of a single AsAd board. The 4×64-channel input connectors to be coupled to the detector are located at the top of the figure. The lower part shows the central VHDCI connector used to send the data to and receive clock information from the concentration boards as well as the connector for powering the board.

A pulse generator embedded on the AsAd board provides voltage steps for tests and calibration purposes. Several modes can be configured to send the generator signal to the input capacitors in order to inject charge on selected channels of the AGET chips. The pulse generator can be triggered either from slow control (programmed pulse sequences) or from an external source on an inspection line. The ADC operating temperature, voltage and current consumption are also monitored on the board. If user-defined limits are exceeded, the AsAd switches to an automatic protection mode and sends alarm signals. The inspection lines can also be used to monitor most of the AsAd digital signals. For optimal use, appropriate steps should be taken to ensure that the cards are properly grounded and shielded from sources of electromagnetic radiation.

3.4. Bus standard: the MicroTCA architecture

Given the relatively large number of channels that were envisioned for the GET system, the choice of bus standard was guided by several requirements. The number of cable bundles and external point-to-point contacts had to be reduced as much as possible to improve the overall robustness of the system since connections are fragile and typically show the first signs of ageing. This excluded the NIM (Nuclear Instrumentation Module) standard. A second requirement was to maximize the data rate from parallel and simultaneous communications from the individual modules of the system. Parallel bus standards, such as VME and VXI, have known limitations even when multiple processors share the same bus. Additional criteria such as the scalability of the system, the portability of the hardware and coupling the system to existing standards were also seen as important factors in the selection of a bus standard for the GET system.

Many of these requirements have already been incorporated in modern telecommunication architectures such as the Micro Telecom Computing Architecture (MicroTCA). In a MicroTCA chassis, communication between slots is uniquely achieved via the backplane, which is based on a dual star topology. In telecommunication applications, this feature significantly reduces the number of cables and provides redundancy in the event of hardware failure. Because the MicroTCA standard was developed by the telecom industry, its performances in terms of overall data throughput and parallel communication capabilities are ideal for our requirements. One of the challenges in this project was therefore to adopt and apply this standard, a previously unknown architecture in

Fig. 5. Photograph of the CoBo. The front panel consists of 4 VHDCI connectors to connect up to 4 AsAd cards, 4 configurable LEMO connectors, and a micro-USB interface for monitoring. The CoBo conforms to the MicroTCA.0 R1.0 PICMG double-width full-height standard.

our community, to the nuclear physics domain. Additional information on the MicroTCA shelf standard can be found in Ref. [35].

For most of the GET tests (Section 4) and detectors (Section 5) described below, users have purchased the MicroTCA chassis from Vadatech (model VT893), the 1 kW power supply (part UTC-010) and the MicroTCA Carrier Hub (MCH) network switch (part UTC-002).

3.5. CoBo: concentration board

The concentration board (CoBo), is a MicroTCA compatible module (custom PCB and firmware package) developed for the GET system. Up to 4 AsAds can be connected to a single CoBo and thus one CoBo module can process data from as many as 1024 signal channels.

There are two communication paths for CoBo, the data path and the control path. The data path processes the raw serialized digital data coming from the AsAd boards and sends the resulting hit-channel registers and multiplicity values to the trigger module (described below in Section 3.6) to generate a master trigger decision. The data are also sent via the MicroTCA backplane through an Ethernet link to external computers for data analysis and storage. The control path uses a dedicated Ethernet connection through the backplane to control and configure CoBo as well as to transmit configuration parameters to the individual AsAd boards. Using the same Ethernet network, it is also possible to configure the MicroTCA compatible Intelligent Platform Management Interface (IPMI) controller to monitor the status of each CoBo board even if it is not programmed or flashed.

The CoBo utilizes the Xilinx Virtex-5 system-on-chip which contains an FPGA and dual PowerPC440 CPU cores. When the GET project began, the Virtex-5 was the best available chip in terms of overall performance and its characteristics were well suited to our application. More modern chips are now available that are being integrated onto GET-compatible hardware for future projects (see Section 6). The CoBo was designed to consume a maximum of 35 W out of the 80 W provided to each slot by the 1 kW power supply in the MicroTCA chassis.

There are multiple clock sources on CoBo, the most important being the Global Master Clock (GMC) provided by the trigger module through the MicroTCA backplane. Both modules are responsible for compensating the differences in phase (due to different trace lengths on the backplane) in a single chassis. Consequently, CoBo provides a synchronization mode that is automatically engaged at boot up. Upon completion of this synchronization step, CoBo runs in normal mode where the GMC is fed into a local PLL and jitter cleaner. The PLL provides 11 differential clock outputs with 123 fs RMS jitter performance. All output frequencies and phases are programmable to further extend the flexibility of the system. The main clock outputs are the write clock frequency for the AGET (adjustable between 1 MHz and 100 MHz), the read clock for the AGET (25 MHz), and the FPGA clocks used for calibration purposes (with values equal to write, read and 100 MHz).
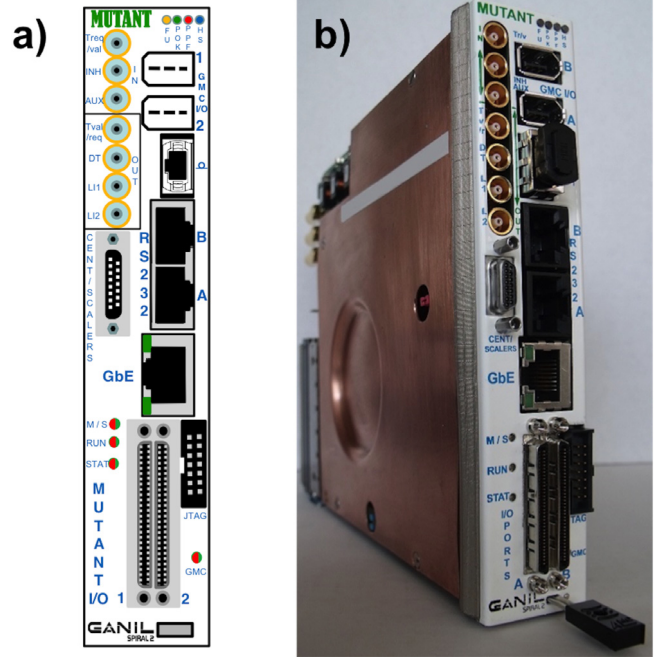

Fig. 6. (a) MuTanT front panel and (b) photograph of the MuTanT module. The MuTanT consists of 2 separate cards housed within a single MicroTCA-compatible module.

The CoBo front panel (Fig. 5) has four programmable input/output LEMO-type connectors, a micro-USB interface, status indicator lights, and four standard Very-High-Density Cable Interconnect (VHDCI) 68-pin connectors, one for each AsAd card. The longest VHDCI cables that have been tested to date are 10 m. The CoBo firmware implements an auto-calibration method to align the ADCs fast-bit clock with the incoming data. The ADCs on the AsAd cards send data at a maximum rate of 4.8 Gb/s (or 1.2 Gb/s/AsAd) during readout. These data are buffered in the CoBo and transmitted at 1 Gb/s via a 10 Gb Ethernet switch on the MCH.

In terms of the overall CoBo system performance, when reading all 512 time bins from all channels (including the 4 FPN channels/AGET) from 4 AsAd cards (full readout of 1088 channels), it takes 1.44 ms for the full data transfer until the system is ready for the next event. The live time of the GET system is described in Section 4.2 and 4.3.

3.6. MuTanT: Multiplicity Trigger and Time

The Multiplicity, Trigger and Time (MuTanT) is a module that serves four principal functions. The MuTanT distributes and manages the GMC of the GET system, it serves as the master/slave shelf interface for single/multi-chassis configurations, it controls the slow control distribution and data readout and it provides a unique three-level trigger system. Due to the complexity of this module, it was designed on two separate cards that are housed within a single-wide MicroTCA compatible module. The first card consists of a Xilinx Virtex-5 PowerPC440 processor and time-to-digital converter (TDC) chip that are primarily dedicated to the management and distribution of the 100 MHz GMC. Clock alignment between the MuTanT and all CoBo modules operating within the same MicroTCA chassis can be performed with a precision of 300 ps (or 500 ps across multiple chassis). The second card is equipped with a second Xilinx Virtex-5 FPGA and is dedicated to the trigger and event time-stamp engine. A detailed schematic of the MuTanT front panel and a photograph of the module is shown in Fig. 6. Additional details and specifications of MuTanT can be found in Ref. [35].

The MuTanT front panel (see Fig. 6) has 7 LEMO connectors that accept and output NIM-type logical signals. Three of these are inputs

and are used for (i) an external trigger request, (ii) an optional trigger inhibit and (iii) an optional multi-purpose input whose function depends on the trigger mode. Two are outputs that are used to send (iv) a fast trigger accept signal and (v) the system dead time. The remaining two outputs are programmable logical inspections. Two additional logical inspections and a GMC output are located at the back of the module. The MuTanT design also includes a dedicated front-panel CENTRUM interface [36] that allows the GET system to be coupled to external data-acquisition systems using the CENTRUM protocol. For other types of data-acquisition systems, a dedicated intermediate card would need to be developed. One example is the MICROTCA compatible module called the Back-End Adaptor for Synchronization of Timestamps (BEAST) that is presently being developed to couple GET with the system originally developed for the Advanced Gamma-ray Tracking Array (AGATA) [37].

The MuTanT has three trigger levels. Level 0 is an external signal that can be input via the front-panel. The external trigger could be derived from an ancillary detector such as a silicon or γ-ray detector operating in or around the TPC volume, for example. Level 1 is an internal multiplicity trigger derived from within the TPC itself. The trigger decision is obtained from a digital sum, at the MuTanT level, from the individual multiplicity sums derived independently from each of the CoBo cards. Two different thresholds (low and high), the time duration in which the multiplicity value remains above or below these thresholds and logical combinations (low, high, low or high, low and high) are all fully programmable in firmware. For decay experiments, where the AGET analog memory is divided into two halves, the L1 trigger can also be split into an L1A (implant) and L1B (decay) trigger with the latter being able to validate or suppress the former. The Level 2 trigger is a software level trigger that relies on the PowerPC440 embedded system. Based on the 64-bit hit pattern from each AGET, a pad/channel matrix can be generated at the MuTanT level. Users can program their own algorithm to select or reject specific events from this hit-pattern matrix. This option could be used, for example, to select or remove events with a unique kinematic signature that would only be expected to occur within a particular geometric region of the detector and that could not be efficiently discriminated using an external trigger (L0) or the total multiplicity (L1) of the system. The three trigger levels (L0, L1 and L2) can be used independently or in a logical AND combination.

Once the event is validated and a trigger is generated, MuTanT then assigns a 32-bit event number and an absolute 48-bit time stamp with a precision of 10 ns. The event number and time stamp are broadcast to all CoBo cards and the full event data are then read out over the MICROTCA backplane and transmitted via the Ethernet MCH uplink output.

3.7. CoBo standalone operating mode

For specific applications requiring a single CoBo ($\leq$ 1024 channels), it is possible to operate the GET system without a MuTanT module. In CoBo standalone mode, an on-board 100 MHz clock is used in place of the GMC provided by the MuTanT. The trigger for the CoBo is then derived independently from the MuTanT from various sources that are selectable in software. External triggers can be sent to one of the LEMO connectors on the CoBo front panel, or internal triggers can be derived from the multiplicity signal generated from all of the AGET chips connected to this CoBo. Another mode allows the standalone system to trigger from the AsAd pulser, which can be useful for calibration purposes and testing. Operating several CoBo cards independently in standalone mode is also possible. However, it is important to emphasize that the samples and time stamps recorded in the different CoBos are not synchronized because they each use independent clocks. A common external trigger must be used for all CoBo cards operated in this mode so that the events can be synchronized offline using the event number.
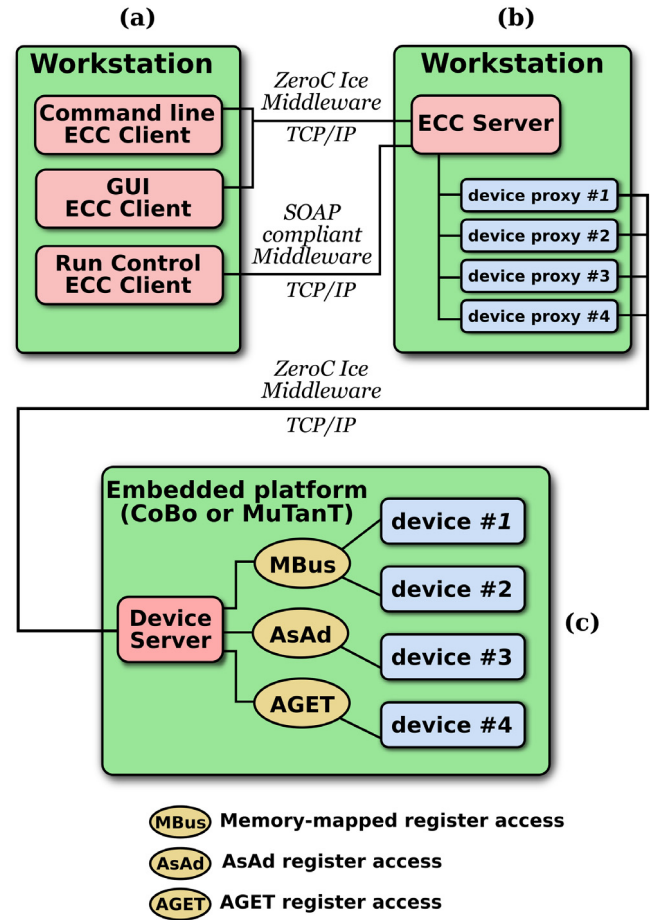

Fig. 7. Schematic overview of the GET ECC server.

3.8. Data-acquisition software

The GET data-acquisition system collects the time-stamped event data from MuTanT and CoBo modules and sends them as a TCP/IP stream to one or several computers operating under Linux. The data-acquisition software consists of three essential subsystems that manage the electronics configuration and control, the data flow and the run control.

The electronics control core (ECC) subsystem, shown schematically in Fig. 7, manages the initialization and monitoring of the electronics boards. Slow control communication to the electronics uses the Internet Communications Engine (ICE) framework [38] with server programs (hwServer) embedded on the MuTanT and CoBo modules. The ECC is used to load the user-defined configuration onto the electronics boards. These operations are initiated via a run control interface (see below) and are transmitted to the ECC through a Simple Object Access Protocol (SOAP). Monitoring the electronics temperatures, voltages and currents (and generation of possible error messages) is achieved through the ECC via SOAP messaging.

The data flow subsystem collects the data from the electronics cards and writes them to disk. This system is based on the existing NARVAL modular data-acquisition framework [39]. The NARVAL system consists of a user-defined set of processes that are called "actors". Dedicated NARVAL actors have been developed for data collection from the electronics cards, event building and merging, data processing and filtering, data broadcasting and data storage. The broadcasting or "watcher" actor, for example, serves as a valuable interface for viewing spectra online.
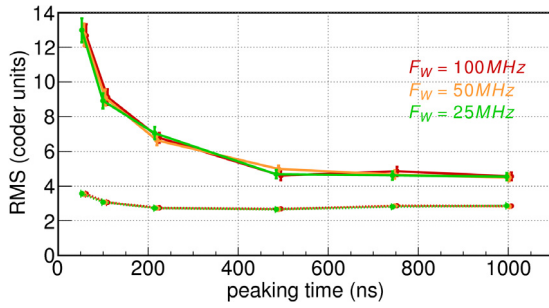
Fig. 8. Average output amplitude fluctuations (RMS) measured for the baseline (no input signals) of a single AGET channel with 120 fC dynamic range and at several peaking times and write frequencies (F_W). The dashed curves show the intrinsic noise measured when the AsAd inputs were not connected. Solid curves show the noise level when the AsAd inputs were connected to the ACTAR TPC demonstrator [3]. Uncertainties reflect the statistical fluctuations from the number of test events.

The run control system orchestrates the ECC and data-flow subsystems using a user-friendly graphical interface. Users can start and stop runs, decide whether or not to save the data to disk, load their particular electronics configuration, observe system status messages and modify the specific topology of the data flow system. The overall system state (ready, running, idle or offline) is indicated and, when the system is running, the data rates at each branch of the data flow are indicated. The run control is the primary interface between the user and the GET system.

4. GET system tests

In this section, measured performances of the system in terms of noise levels, data throughput and system live time are described in detail.

4.1. Baseline mean and noise

Uncorrected baseline means and standard deviations for a single AsAd card whose inputs were not connected to a detector are presented in Ref. [34]. For a peaking time of 502 ns, the average standard deviation of the intrinsic baseline noise was found to be between 3 and 4 ADC units. This was improved to ~2.2 ADC units after applying corrections for the baseline shape. Once the AsAd inputs are connected to a detector, results will vary according to the capacitance of the particular system but the majority of detector projects have achieved baseline standard deviations of 3 to 5 ADC channels after applying the corrections described in Ref. [34]. An example of how the noise varies with the peaking time, the writing frequency and the influence of coupling the electronics to a detector is presented in Fig. 8.

4.2. Data throughput

For every event, each CoBo sends one data frame per AsAd card. The format of these data frames depends upon the readout mode selected. In the standard format, used in partial readout mode or when the zero suppression feature is enabled, each sample value requires 4 bytes. Readout of all 512 time bins from a single channel thus corresponds to 2048 B while the readout of all channels from a single AsAd card (256 data channels + 16 FPN channels) requires 557056 B. In full readout mode, a more compact data-frame format with only 2 B per sample is used that requires 278528 B for all channels from a single AsAd card. An additional 256 B is reserved, in both formats, for the data frame header.

Tests of the overall data rate and throughput of the GET system were performed using a complete hardware configuration that consisted of

1 MuTanT, 2 CoBos and 8 AsAd cards. The MuTanT and CoBos were operated in a Vadatech VT893 MicroTCA chassis. A direct 10 Gb/s optical fibre link was used to connect the MCH in the chassis to a 10 Gb network adapter on the data-acquisition computer. The acquisition computer was a Dell PowerEdge R420 server with dual 6-core/12-thread Xeon E5-2430 2.2 GHz processors and 32 GB of RAM. The acquisition network was configured to use jumbo frames with the maximum transmission unit set to 8000 B. The acquisition was triggered using an external pulser and data from all 8 AsAd cards were read in full readout mode. In the results presented below, data were not written to disk and measured data rates were not limited by the computer.

A periodic external pulser signal with an adjustable frequency was used to trigger the system. With this configuration, a maximum data rate of 850 Mb/s on each CoBo at a pulser frequency of 100 Hz was achieved. At this rate, approximately 95% of the trigger requests (or 95 triggers/s) were accepted. At a pulser frequency of 80 Hz, the data rate was 715 Mb/s per CoBo and the accepted trigger rate was 100%. A full characterization of the system live time using a random pulse generator is described in Section 4.3.

The maximum data rate of 850 Mb/s per CoBo achieved in full readout mode corresponds to an event rate of 380 Hz with a single AsAd card connected to the CoBo or 95 Hz with all 4 AsAd cards connected to the CoBo. These data rates have been confirmed in similar tests performed by several other users of the GET system. It should be emphasized that experiments would likely never be able to record to disk the amount of data generated at this maximum rate. In most applications, only a small fraction of the total number of channels are hit and thus the system will typically be operated in partial readout mode. Selecting only the hit channels will drastically reduce the amount of data to be recorded on disk. The data volume can be further reduced by activating the zero-suppression threshold that is adjustable on a channel-by-channel basis.

4.3. System live time

Measurements of the system live time were performed using the same configuration of 8 AsAd cards as described in the data throughput tests of Section 4.2. In these tests, a random pulse generator (Berkeley Nucleonics Corporation model DB-2) was used to simulate a real experiment and was input as an external trigger to MuTanT. The mean frequency of the pulser was adjusted from 100 Hz up to 16 kHz and channels were read in partial readout mode. The number of channels read was varied in order to characterize the live time of the system over a wide range of counting rates. For each channel, all 512 time bins were read and given the fixed read frequency of 25 MHz, the time required to read each channel is therefore 20.48 μs.

Results presented below are for a single AGET chip. The dead-time-per-trigger-event was measured from the width of the dead-time output signal that is available on the front panel of the MuTanT module. The measured dead time as a function of the number of channels read is shown in Fig. 9 where the black circles are the measured data points and the red line corresponds to a linear fit. The offset of 52.4 μs measured for this particular AGET chip is the overhead required to start the read process. The slope of 20.5 μs/channel is in perfect agreement with the time required to read 512 time bins at 25 MHz. For all 68 AGET channels (64 data channels plus 4 FPN channels), the system requires 1.44 ms to process each event. This processing time scales with the number of time bins read. If, for example, only half of the 512 time bins were read for every channel then dead-time-per-event would be reduced by a factor of 2.

By varying the frequency of the random pulser, the overall live time (in %) of the system was characterized as a function of the number of channels read. For each measurement (circles in Fig. 10), a particular number of channels was selected and for every channel selected, all 512 time bins were read for every trigger event. The measured live time was obtained from the ratio of the number of accepted triggers (trigger
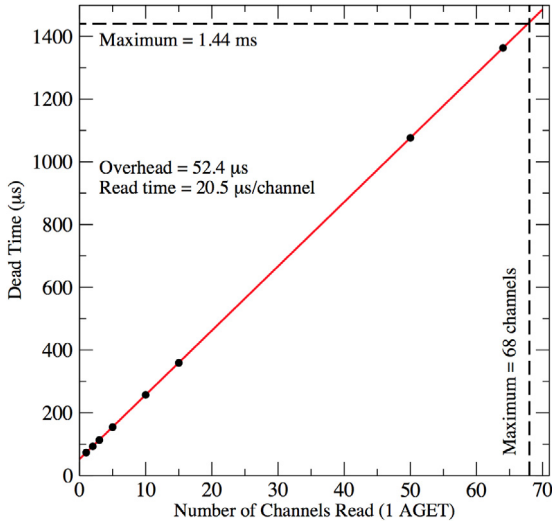
Fig. 9. Measured dead time (black circles) for a single AGET chip as a function of the number of channels read. A linear fit to these data (red line) resulted in an overhead (offset) of 52.4 μs and a slope of 20.5 μs/channel. Both are a function of the fixed reading frequency (25 MHz) and the number of time bins read per channel (512).
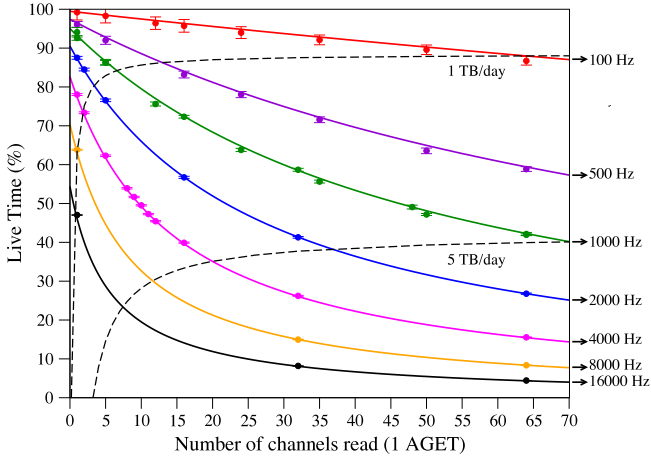

Fig. 10. Measured live time as a function of channels read for a single AGET chip. All 512 time bins were read for every channel. The solid curves are the statistical expectations based on the Poisson probability distribution and a fixed and constant dead time per event. The dashed curves indicate what these rates correspond to in terms of the total amount of data collected (1 TB/day and 5 TB/day).

accept signal from the MuTanT front panel) to the number of requested triggers (the total number of pulser signals). Each measurement lasted 60 s in duration.

For a fixed number of channels read, the dead-time-per-event is a constant (non paralyzable) and depends only on the number of channels according to Fig. 9. If this constant dead-time per event is τ, then the live-time fraction L of the system for a pulser with a frequency R can be written as [40]:

$$L = \frac{1}{1 + R\tau}. \tag{1}$$

This expression was used to generate the solid curves in Fig. 10 that are in excellent agreement with the measured results. With this simple equation, that depends only on the number of channels read and the desired trigger rate, users can quickly and reliably estimate the live time of the GET system for their particular application. When performing these calculations, one also has to consider the total amount of data that will be generated. The dashed curves in Fig. 10 indicate an overall data collection of 1 and 5 TB/day from a single AGET chip. Reading only
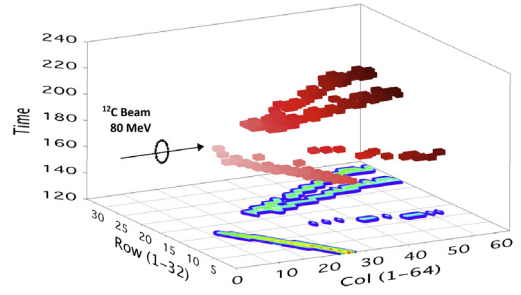

Fig. 11. Reconstructed ^{12}C + $\alpha \rightarrow 4\alpha$ breakup event with the ACTAR TPC demonstrator. The images on the grid at the bottom of the plot are the 2 dimensional charge collected on 2×2 mm^2 pads. In red, the timing information from the individual pads is used to reconstruct the event in 3 dimensions. The 4 alpha particles (3 from the breakup of ^{12}C and one from the recoiling He in the gas) are visible. (For interpretation of the references to colour in this figure legend, the reader is referred to the web version of this article.)

a fraction of the AGET memory (rather than the full 512 time bins) or activating zero-suppression can be used to reach higher counting rates and decrease the amount of data.

When channels are spread over multiple AsAd cards, the system live time in partial readout mode will be limited by the AGET with the largest number of hit channels (Fig. 9). For example, if all 68 channels are active on a single AGET the dead time per event will be 1.44 ms (with all 512 time bins read per channel). Activating an additional 30 channels on a second AGET will not increase the system dead time even though more total channels are being read. Activating more and more channels will, however, eventually meet or exceed the 850 Mb/s maximum rate of the CoBo. Distributing channels across several AGETs should therefore be carefully considered when designing the detector-to-channel routing.

5. Detectors and projects employing the GET system

In this section we introduce some of the detector projects currently using the GET system and present some of their preliminary results.

5.1. ACTAR TPC — Europe

The Active Target and Time Projection Chamber (ACTAR TPC) project is financed through a research starting grant awarded by the European Research Council (ERC) [41]. Physics cases are focused on the study of nuclei furthest from stability using direct reactions and exotic nuclear decays. Experiments will be performed at GANIL, ISOLDE and rare-isotope beam facilities worldwide. The project will construct two distinct detectors with identical technical and mechanical solutions but with different physical geometries in order to optimize the detector design towards the wide range of kinematics and beam energies (typically between 5 and 100 MeV/u) that are required by the broad physics program. The two geometries will be cubic and cuboid where the pad-plane geometries are square (256×256 mm^2) and rectangular (128×512 mm^2), respectively. In both geometries, the pad plane will consist of micro-pattern gaseous detectors coupled to square pads with a pitch of 2×2 mm^2 [42]. Both geometries will have a total of 16384 channels. One set of GET electronics will be used interchangeably between the two detectors. First experiments with ACTAR TPC are anticipated in 2018.

Before the final construction, the ACTAR TPC collaboration built a 2048-channel "demonstrator" version of the final design [3]. In Fig. 11, a sample event is shown from a recent in-beam experiment that was performed at the tandem accelerator of the ALTO facility at IPN Orsay. A beam of ^{12}C at 80 MeV was sent into the demonstrator that was filled with a gas mixture of He:iC$_4$H$_{10}$ (95:5) with a total pressure of 1000 mbar. In Fig. 11, the ^{12}C enters from the left side of the figure (rows 15–17) where it breaks up into 3 alpha particles. The figure clearly shows the trajectories of the 4 alpha particles (3 from
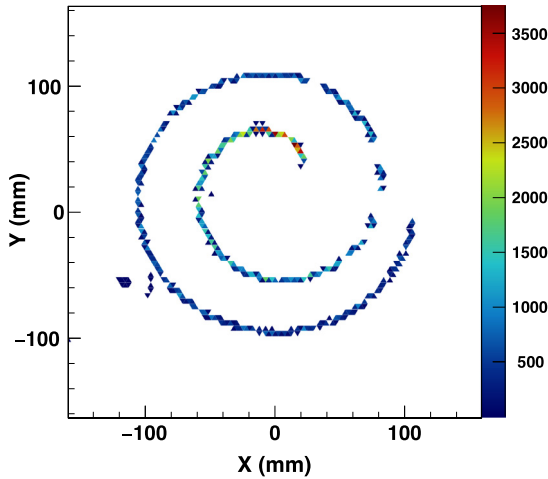
Fig. 12. Charge projection of the helical trajectory of recoil proton in the AT-TPC from the elastic scattering of an ^{46}Ar beam at 4.5 MeV/u in iC$_4$H$_{10}$ gas at 20 Torr pressure and surrounded by a magnetic field of 2 T.

Fig. 13. Single event recorded with the SπRIT TPC following the reaction of a ^{132}Sn beam accelerated to 270 MeV/u on a solid ^{124}Sn target located at the entrance to the detector ($x = 0$, $z = 0$). Several light ions are produced whose trajectories are slightly curved in the magnetic field. In this event, a pion was also produced as evidenced by the spiral trajectory in the upper half of the figure.

the breakup of ^{12}C and 1 from the recoiling He in the gas) as they travel through the detector. The ^{12}C beam is not visible in Fig. 11 as a passive aluminium foil was used to cover the central rows and prevent the electrons produced from the unreacted ^{12}C beam from reaching the amplifier.

5.2. AT-TPC — United States

The AT-TPC is a cylindrical active target that was designed and constructed at the National Superconducting Cyclotron Laboratory (NSCL). The detector is housed inside a 2 T superconducting solenoid magnet and will be used for experiments with beam energies of up to 6 MeV/u at the re-accelerator facility ReA3 at NSCL. The AT-TPC design was scaled from a smaller and non-magnetic prototype, the PAT-TPC [43] that has been recently used to study resonant α-particle scattering [44–46]. The drift volume of the AT-TPC is 100 cm in length and is oriented parallel to the beam axis. A circular readout pad plane with a diameter of 50 cm is located at the end of the chamber and is perpendicular with respect to the beam axis. The pad plane is segmented into 10240 triangular shaped pads with two different sizes. Small triangles, with side lengths of 1 cm, are used in the inner 30 cm diameter (closest to the beam axis) while large triangles, with side lengths of 2 cm, are used in the outer diameter (> 30 cm). The use of smaller pad sizes close to the beam axis is to improve the position determination of the reaction vertex. The longitudinal magnetic field induces the emitted charged particles to follow helical orbits in the TPC that is crucial for particle identification and energy measurements as well as increasing the overall path length in which the particles can be tracked. A typical event from the interaction of an ^{46}Ar beam at 4.5 MeV/u with iC$_4$H$_{10}$ gas at 20 Torr that shows the projection of the helical orbit of the scattered recoil proton on the pad plane is presented in Fig. 12.

5.3. SπRIT — Japan

The SAMURAI Pion-Reconstruction and Ion Tracker (SπRIT) TPC [4] was developed for use inside the SAMURAI superconducting dipole magnet [47] at the RIKEN Radioactive Isotope Beam Factory (RIBF). The main aim of the device is to study the density dependence of the nuclear symmetry energy through heavy-ion collisions of neutron-rich nuclei at incident energies of up to 350 MeV/u. The SπRIT TPC employs Multi-Wire Pad Chamber (MWPC) wire amplification planes that are situated below a cathode-pad readout plane that is segmented into 8 × 12 mm^2 rectangular pads. A total of 112 × 108 pads cover the active area of
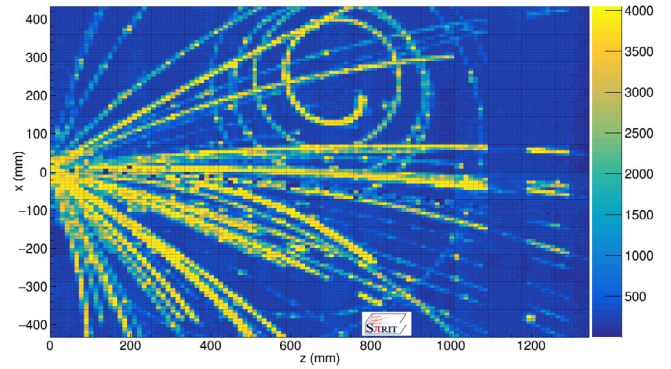
the readout plane. The dimensions of the active volume of the TPC are 89.6 cm in width, 129.6 cm in length (parallel to the beam axis) and 50 cm in height (direction of the electron drift). The detector operates inside a magnetic field of 0.5 T and is typically filled with 1 atm of P10 gas (90% argon, 10% methane). The 12096 channels of SπRIT are read using 48 AsAd boards, 12 CoBo boards, 2 MuTanT modules, and 2 MicroTCA chassis. Weakly-ionizing signals from pions and light-charged particles (protons) require the maximum electronics gain of 120 fC. A single event from the ^{132}Sn+ ^{124}Sn reaction is presented in Fig. 13.

5.4. CHIMERA and FARCOS — Italy

The GET electronics will also be employed for several non-TPC detector applications including the caesium-iodide scintillation detectors and silicon strip detectors used in the CHIMERA and FARCOS (Femtoscopy Array for Correlations Spectroscopy) Si-CsI(Tl) telescopes [7,48–50]. The physics programs require a large dynamic range of more than 10^3. The use of the existing CHIMERA pre-amplifiers [51] is mandatory to achieve this. Output signals from these external pre-amplifiers will be sent to GET and bypass the pre-amplification stage of the AGET.

The electronics and data acquisition system previously developed for the CHIMERA silicon detectors (based on VME) will continue to be used. The NARVAL framework (described above in Section 3.8) will synchronize and merge the data flow coming from the CHIMERA and GET systems based on the GMC from MuTanT. The master trigger will be derived from the overall multiplicity of the Si strip detectors, which is typically very low (from one to several strips) compared to TPC applications. Successful test results have already been obtained when triggering the GET system internally (L1) with only a single hit channel. To achieve this, shielding the AsAd cards and the inputs of the AGET chips was essential in order to reduce the noise.

Tests of the GET system with silicon detectors were performed using a 300 μm thick, 64 × 64 mm^2 double-sided silicon strip detector with 32 strips on each side. A new external ASIC-based pre-amplifier that was specifically developed for FARCOS was used [52]. Various digital filters were tested in order to improve the signal-to-noise ratio and the resolution. The best results were obtained by subtracting, on an event-by-event basis, the noise signals derived from the FPN channels and applying a triangular filter to the baseline restored signals before searching for the maximum amplitude of the signals. A typical α-particle energy spectrum obtained from a mixed source of ^{239}Pu, ^{241}Am and ^{244}Cm is shown in Fig. 14a). An energy resolution of about 60 keV (FWHM) is routinely achieved with GET. For comparison, an energy resolution of 25 keV (FWHM) was obtained with this same detector using a commercial 14-bit fast digitizer operating in VME.
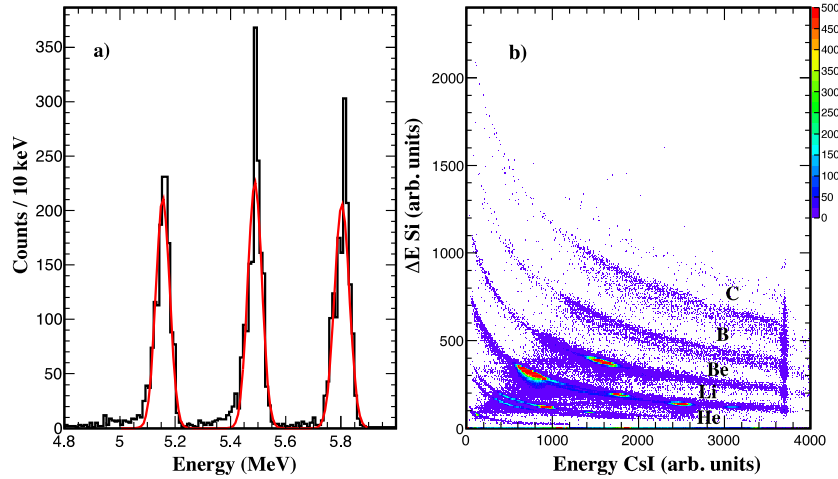
Fig. 14. (a) Typical α-particle energy spectrum obtained from a mixed source of ^{239}Pu, ^{241}Am and ^{244}Cm with a 300 μm thick double-sided silicon strip detector coupled to GET. (b) Particle identification plot obtained from the energy-loss deposited in the silicon versus the remaining energy deposited in the CsI detector of a CHIMERA telescope. Data were obtained from a cocktail beam fragmented on a light target.
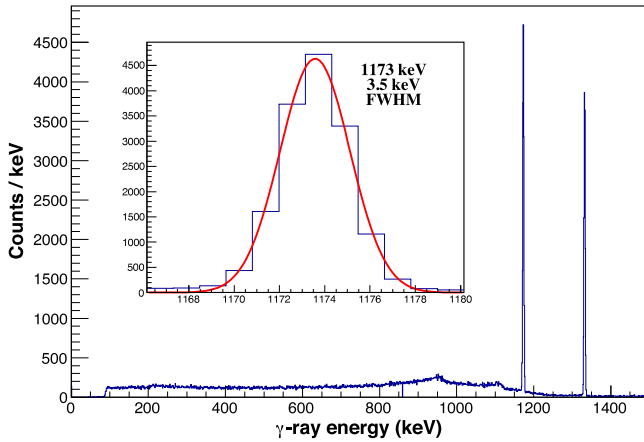

Fig. 15. Singles γ-ray energy spectrum from a ^{60}Co calibration source measured with a coaxial HPGe detector coupled to the GET system. Following a detailed analysis of the baseline shapes using the FPN channels (see text), an energy resolution of 3.5 keV (FWHM) was achieved for the 1173 keV γ-ray.

A particle identification plot obtained with the GET system is presented in Fig. 14b). Data were obtained from a mixed beam of ^{10,11}Be, ^{13}B and ^{16}C produced from projectile fragmentation of an ^{18}O beam accelerated to 55 MeV/u on a Be target at the In Flight Radioactive Ions Beams (FRIBs) facility of the INFN-Laboratori Nazionali del Sud (LNS) in Catania, Italy. The vertical line at channel ~ 3700 is due to saturation of the dynamic range for the CsI detector at this particular gain setting. The resolution obtained is clearly sufficient for separating isobars up to carbon.

5.5. HPGe detectors — Italy

Measurements of the GET system have been recently performed using a cylindrical (58 mm diameter, 63 mm length) coaxial high-purity germanium (HPGe) detector (ORTEC GMX-30200-P) at Messina University in Italy. Pre-amplified signals from the HPGe detector were sent to the Sallen–Key low-pass filter stage of the AGET with 502 ns peaking time. Using a ^{60}Co calibration source an energy resolution of 3.5 keV (FWHM) was obtained for the 1173 keV γ ray. A γ-ray singles spectrum is presented in Fig. 15. This can be compared to about 2.5 keV (FWHM) previously obtained with this detector using an ORTEC 572 spectroscopy amplifier and a standard 14-bit ADC. Since

the intrinsic noise of the HPGe is considerably less than Si, the energy resolution obtained with GET could only be achieved once a full and detailed analysis of the baseline shape was performed using the data from the FPN channels. Without such an analysis the energy resolution obtained was only 7 keV (FWHM). This result highlights the importance of these channels for analysing high-resolution spectral data.

5.6. LaBr$_3$ scintillating detectors for SpecMAT — Belgium

The SpecMAT active target [13] is presently being built at KU Leuven. The detector will consist of a cylindrical time projection chamber that will be placed inside a solenoid magnet to study low-energy nuclear reactions. The base geometry is similar to the AT-TPC described in Section 5.2. The unique aspect of this project is that the TPC will be surrounded by an array of scintillating detectors to perform coincident γ-ray spectroscopy. The entire detection system will be operated in magnetic fields of up to 3 T. A prototype 1.5″ cubic LaBr$_3$:Ce detector coupled to a SensL C-series silicon photomultiplier array (SiPM model 60035-64P-PCB) was tested using the GET system. To match the crystal size, only the inner 6×6 SiPMs out of the entire 8×8 array were biased and read out. All energy output signals of the active SiPMs were summed and amplified in a custom adaptor board before being sent to the gain-2 stage of the AGET chip (bypassing the internal pre-amplification and filter stages in the AGET). Samples of digitized waveforms obtained with 100 MHz sampling rate in GET are shown in Fig. 16. The γ-ray energy was reconstructed using the maximum amplitude (pulse height) of the signals after applying a baseline subtraction. The baseline was determined on an event-by-event basis using an average of the 15 time buckets immediately preceding the start of the signal. The resulting γ-ray energy spectrum is presented in the bottom panel of Fig. 16. This spectrum is compared to the result obtained from the same detector coupled to a conventional analog system using a Canberra 8715 ADC. A summary of the energy resolutions obtained with these two systems is provided in Table 3. The results obtained with the GET system are already very encouraging and are expected to be further improved once a more detailed study of the FPN channels is included into the waveform analysis.

5.7. Other projects using GET

In addition to the projects described above, the GET system has been adopted for a large number of similar devices as summarized in Table 1. The system is being used for a wide range of applications including silicon, caesium-iodide and lanthanum-bromide scintillating detectors

Table 3

Comparison between the energy resolutions obtained from a LaBr$_3$:Ce detector coupled to the GET system and to an analog system using standard γ-ray calibration sources of ^{60}Co and ^{137}Cs.

γ-ray energy (keV)	Energy resolution (%,FWHM)	
	GET	Analog
662	3.99	3.49
1173	3.31	2.60
1333	2.44	2.47
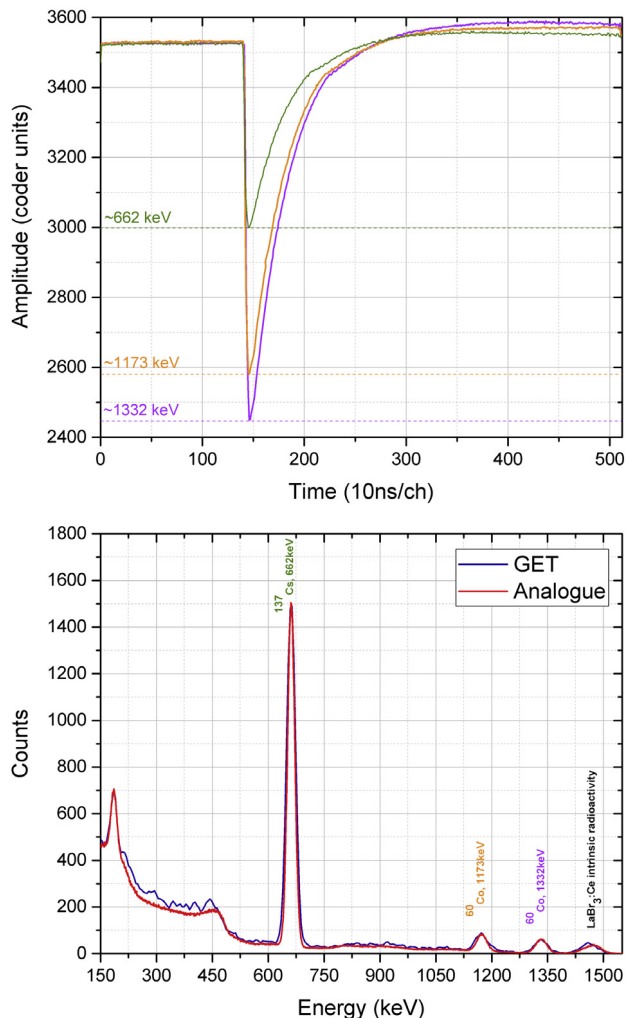
Fig. 16. (Top) Digitized energy signals from a LaBr$_3$:Ce detector coupled to the GET system. The three signals correspond to the 662 keV γ ray from a ^{137}Cs calibration source and the 1173 and 1333 keV γ rays from a ^{60}Co source. (Bottom) Comparison of the γ-ray energy spectrum obtained with the GET system and a conventional analog system. The analog spectrum (red) was normalized to the GET spectrum (blue) since it contains significantly more counts. (For interpretation of the references to colour in this figure legend, the reader is referred to the web version of this article.)

and with a micromegas neutron beam profile monitor [8] at CERN's neutron time-of-flight (nTOF) facility. The GET system will also be used to equip a set of gas-filled beam tracking detectors at the future Super Separator and Spectrometer (S^3) facility at GANIL/SPIRAL2.

6. Extensions to the GET system

The GET project was originally motivated by the requirements of three relatively large-scale instruments in nuclear physics (ACTAR TPC, AT-TPC and SπRIT TPC). However, throughout the design phase of the project, we were aware of similar electronics needs within the community. The system was therefore designed to cover as wide a range of applications as possible given the available resources. Today, the result is that the number of GET users and total number of channels deployed (see Table 1) have, by far, exceeded our expectations. Through this momentum, a number of extensions have already been funded while others are being evaluated. A brief description of the orientation for possible future extensions is listed below:

(i) A number of projects require extending the dynamic range through the use of external pre-amplifiers and filters. These circuits will also include handling charges that saturate the extended dynamic range. Pre-amplifiers with ASIC chips are being built. Through these projects, the system will cover an even wider range of detector types including photo-multipliers and solid-state devices.

(ii) To secure future modifications of the code and to introduce new functions, the firmware is being recast using a fully generic approach.

(iii) To extend the digital memory and longevity of the CoBo modules, the latest FPGA chips are being integrated onto CoBo-like hardware. This will replace the Xilinx Virtex-5 on the present CoBo with next generation chips such as the Zynq family.

(iv) A back-end module called BEAST (Section 3.6) is being developed to synchronize time stamps from multiple data acquisitions. This will allow the GET system to be coupled to an even wider range of external data-acquisition systems.

(v) To cover the needs of instruments with relatively few channels (≤ 64) a card called the Single AGET Module (SAM) is being built that will integrate the CoBo functions onto the front end.

7. Summary and conclusion

In this article, a detailed description of the GET hardware, software and firmware is presented. A number of new approaches were developed and realized within a scalable and generic approach. A new ASIC chip with a number of new features, the use of the modern MicroTCA telecommunication hardware and the three-level trigger are some of the main highlights. Given the generic approach, the system has already been employed in a number of applications in nuclear, particle, underground and medical physics. In some of these instruments, data have already been collected and are being analysed. Several specific examples were provided in Section 5.

The GET system is also being deployed as a development tool for new instruments. A large fraction of GET users have developed the necessary tools and analysis techniques to be able to use the system with, for example, solid-state detectors and photo-multipliers. While optimum resolution or dynamic ranges are not necessarily achieved for such applications, these disadvantages are offset by the relatively compact multi-channel geometry, multi-function and resourceful back end. The state-of-the-art multi-level trigger was virtually unknown in the nuclear physics community before the GET project. This will significantly facilitate data capture and minimize unnecessary overhead on the laboratories computing facilities. New additions and extensions to GET will improve the system further.

An important aspect of the entire development is the relatively large number of international users. This alone will ensure that there will be a significant effort in reaching optimal system configurations as well as the sharing of knowledge and expertise. The wide range of applications and the growing number of users highlights both the flexibility of the system and the need for a robust, modern, cost-effective and long-term solution in the nuclear physics community.

Acknowledgments

References

[1] S. Beceiro-Novo, T. Ahn, D. Bazin, W. Mittig, Prog. Part. Nucl. Phys. 84 (2015) 124.
[2] G. Jhang, et al., J. Korean Phys. Soc. 68 (2016) 645.
[3] T. Roger, et al., Nucl. Instrum. Methods Phys. Res. A xx (2017) yyy.
[4] R. Shane, et al., Nucl. Instrum. Methods Phys. Res. A 784 (2015) 513.
[5] W. Mittig, et al., Nucl. Instrum. Methods Phys. Res. A 784 (2015) 494.
[6] S.H. Kim, et al., JPS Conf. Proc. 17 (2017) 033009.
[7] E.V. Pagano, et al., EPJ Web Conf. 117 (2016) 10008.
[8] J. Pancin, et al., Nucl. Instrum. Methods Phys. Res. A 524 (2004) 102.
[9] S. Ota, H. Tokeida, C.S. Lee, Y.N. Watanabe, J. Radioanal. Nucl. Chem. 305 (2015) 907.
[10] J.S. Bihałowicz, AIP Conf. Proc. 1645 (2015) 301.
[11] Zhao Hong-yun et al., private communication.
[12] X. Chen, et al., Sci. China Phys. Mech. Astron. 60 (2017) 061011.
[13] R. Raabe, Spectroscopy of exotic nuclei in a Magnetic Active Target (SpecMAT). https://erc.europa.eu/spectroscopy-exotic-nuclei-magnetic-active-target.
[14] E. Koshchiy, G.V. Rogachev, E. Uberseder, E. Pollacco, Cyclotron Institute Texas A&M University Progress in Research 2015, 2015, p. 242. https://cyclotron.tamu.edu/progress-reports/2014-2015/cyclotron_progress_2015.pdf.
[15] T. Ahn, private communication.
[16] J. Pancin, private communication.
[17] Qian Liu, private communication.
[18] G.D. Alkhazov, et al., Phys. Rev. Lett. 78 (1997) 2313.
[19] Y. Mizoi, et al., Nucl. Instrum. Methods Phys. Res. A 431 (1999) 112.
[20] C.E. Demonchy, et al., Nucl. Instrum. Methods Phys. Res. A 583 (2007) 341.
[21] B. Blank, et al., Nucl. Instrum. Methods Phys. Res. A 613 (2010) 65.
[22] M. Camaaño, et al., Phys. Rev. Lett. 99 (2007) 062502.
[23] I. Tanihata, et al., Phys. Rev. Lett. 100 (2008) 192502.
[24] T. Roger, et al., Phys. Rev. C. 79 (2009) 031603(R).
[25] S. Ilieva, et al., Nuclear Phys. A 875 (2012) 8.
[26] C. Monrozeau, et al., Phys. Rev. Lett. 100 (2008) 042501.
[27] M. Vandebrouck, et al., Phys. Rev. Lett. 113 (2014) 032504.
[28] J. Giovinazzo, et al., Phys. Rev. Lett. 99 (2007) 102501.
[29] P. Ascher, et al., Phys. Rev. Lett. 107 (2011) 102502.
[30] Y. Giomataris, et al., Nucl. Instrum. Methods Phys. Res. A 376 (1996) 29.
[31] F. Sauli, Nucl. Instrum. Methods Phys. Res. A 386 (1997) 531.
[32] F. Sauli, Nucl. Instrum. Methods Phys. Res. A 805 (2016) 2.
[33] P. Baron, et al., IEEE Trans. Nucl. Sci. 55 (2008) 1744.
[34] J. Giovinazzo, et al., Nucl. Instrum. Methods Phys. Res. A 840 (2016) 15.
[35] G. Wittwer, F. Saillant, M. Blaizot, G.F. Grinyer, B. Raine, C. Belkhiria, S. Primault, C. Gueye, Real Time Conference RTC 2014. http://dx.doi.org/10.1109/RTC.2014.7097417.
[36] G. Wittwer, Clock Event Number Transmitter Receiver Universal Module (CENTRUM). http://wiki.ganil.fr/gap/wiki/Documentation/VXI/CENTRUM.
[37] S. Akkoyun, et al., Nucl. Instrum. Methods Phys. Res. A 668 (2012) 26.
[38] M. Henning, IEEE Internet Comput. 8 (2004) 66.
[39] X. Grave, R. Canedo, J.F. Clavelin, S. Du, E. Legay, Real Time Conference RTC 2005. http://dx.doi.org/10.1109/RTC.2005.1547454.
[40] G.F. Knoll, Radiation Detection and Measurement, third ed., John Wiley & Sons, 2000.
[41] G.F. Grinyer, Active Target and Time Projection Chamber (ACTAR TPC). https://erc.europa.eu/active-target-and-time-projection-chamber.
[42] J. Pancin, et al., Nucl. Instrum. Methods Phys. Res. A 735 (2014) 532.
[43] D. Suzuki, et al., Nucl. Instrum. Methods Phys. Res. A 691 (2012) 39.
[44] D. Suzuki, et al., Phys. Rev. C 87 (2013) 054301.
[45] A. Fritsch, et al., Phys. Rev. C 93 (2016) 014321.
[46] T. Ahn, et al., Nucl. Instrum. Methods Phys. Res. B 376 (2016) 321.
[47] H. Sato, et al., IEEE Trans. Appl. Supercond. 23 (2013) 4500308.
[48] A. Pagano, et al., Nuclear Phys. A 734 (2004) 504.
[49] A. Pagano, et al., Nucl. Phys. News 22 (2012) 1.
[50] E. De Filippo, A. Pagano, Eur. Phys. J A 50 (2014) 32.
[51] R. Bassini, C. Boiana, A. Pagano, A. Pullia, IEEE Trans. Nucl. Sci. 51 (2004) 115.
[52] C. Guazzoni et al., private communication.